Available online at www.sciencedirect.com

SciVerse ScienceDirect

Ceramics International 39 (2013) 3087–3094

CERAMICS INTERNATIONAL

www.elsevier.com/locate/ceramint

Increased cycling stability of $Li_4Ti_5O_{12}$-coated $LiMn_{1.5}Ni_{0.5}O_4$ as cathode material for lithium-ion batteries

Yan-Rong Zhu, Ting-Feng Yi*, Rong-Sun Zhu, An-Na Zhou

School of Chemistry and Chemical Engineering, Anhui University of Technology, Maanshan, Anhui 243002, People's Republic of China

Received 25 August 2012; received in revised form 3 September 2012; accepted 26 September 2012
Available online 8 October 2012

Abstract

$Li_4Ti_5O_{12}$ (LTO)-coated 5 V spinel $LiMn_{1.5}Ni_{0.5}O_4$ as cathode was prepared by the sol–gel method followed by high-temperature calcinations. The structural and electrochemical properties of these cathodes were investigated using differential thermal analysis (DTA) and thermogravimetery (TG), X-ray diffraction (XRD), scanning electron microscopy (SEM), cyclic voltammetry (CV), and charge–discharge studies. TG–DTA shows that $LiMn_{1.5}Ni_{0.5}O_4$ spinel forms at about 400 °C. XRD reveals that a substitutional compound $LiMn_{2-x-y}Ni_xTi_yO_4$ can be formed when the coated content of LTO exceeds 3 wt%. SEM exhibits that the coated $LiMn_{1.5}Ni_{0.5}O_4$ is covered with small particles that consist mainly of LTO. CV and dQ/dV versus voltage curves demonstrate that the modified material exhibits remarkably enhanced electrochemical reversibility and stability. The charge–discharge test indicates that 3 wt% LTO-coated $LiMn_{1.5}Ni_{0.5}O_4$ has excellent fast charge–discharge performances. These results reveal that LTO-coated layer protects the surface of the active materials from HF in the electrolyte during electrochemical cycling. As a result, the surface-modification of $LiMn_{1.5}Ni_{0.5}O_4$ with LTO should be an effective way to improve the fast charge–discharge properties.

Keywords: $LiMn_{1.5}Ni_{0.5}O_4$; Cathode material; Coating; Electrochemical performance

1. Introduction

Lithium ion batteries (LIBs) are currently used in a range of portable electronic devices due to their high energy density [1,2]. However, the current commercial lithium-ion batteries commonly based on layered Co oxide positive-electrode materials ($LiCoO_2$) can hardly fulfill the requirement of high power applications. Spinel $LiMn_2O_4$ is of particular interest for use in hybrid electric vehicles (HEVs) and electric vehicles (EVs) as the cathode material for high-power Li-ion batteries because of the low material cost, abundant material supply and better environmental compatibility compared to other cathode materials. However, there are some drawbacks associated with the poor electrochemical performance of $LiMn_2O_4$ cathode material, such as Jahn–Teller distortion [3], manganese dissolution and electrolyte decomposition [4,5]. The first factor could be significantly improved by partial substitution of manganese cations with transition metal like Ni [6], Co [7], Cr [8], Cu [9] and Fe [10]. Among these, $LiMn_{1.5}Ni_{0.5}O_4$ has been studied due to its significant reversible capacity (theoretical value 148 mAh g^{-1}) and high voltage (4.7 V versus Li/Li^+). The high operating voltage and chemical stability of $LiMn_{1.5}Ni_{0.5}O_4$ make it a strong cathode candidate for next generation lithium-ion batteries with high energy density [11]. As the cathode contacted with the Li-based electrolyte directly in Li-ion batteries, Mn or Ni dissolution can be induced by the generation of acids like hydrogen fluoride (HF). This phenomenon results from the reactions of fluorinated anions with the manufacture of unnstable Li-based salt [12] and solvent oxidation [13]. Surface modification was considered as an effective way to reduce the side reactions. The surface treatment of spinel $LiMn_{1.5}Ni_{0.5}O_4$ could decrease the surface area to retard the side reactions between the active material and electrolyte. The coated layer includes ZnO [14], Bi_2O_3 [15], Al_2O_3 [16], SiO_2 [17], Li_3PO_4 [18], carbon [19], and so on. $Li_4Ti_5O_{12}$ (LTO) is a zero-strain material, meaning that there is no structural change during the insertion/extraction

*Corresponding author. Tel.: +86 555 2311807; fax: +86 555 2311822.
E-mail address: tfyihit@163.com (T.-F. Yi).

0272-8842/$ - see front matter © 2012 Elsevier Ltd and Techna Group S.r.l. All rights reserved.
http://dx.doi.org/10.1016/j.ceramint.2012.09.088

of lithium ions [20]. $Li_4Ti_5O_{12}$ has a higher Li-insertion voltage (1.55 V versus Li/Li^+) than that of commercial graphite anode, and then can avoid the reduction of electrolyte on the electrode surface and formation of the solid-electrolyte interphase (SEI) layer (usually occurring below 0.7 V Li/Li^+) [21]. Based on the merits mentioned above, it can be concluded that $Li_4Ti_5O_{12}$ is suitable for the surface modification of cathode materials. Takada et al. [22] reported that $Li_4Ti_5O_{12}$ coatings improved the capacity of $LiCoO_2$. Liu et al. [23] reported that the $Li_4Ti_5O_{12}$-coated $LiMn_2O_4$ material exhibited excellent capacity retention at high temperature. As we know, the storage of electrical energy at high charge–discharge rate is an important technology because this can enable hybrid and plug-in hybrid electric vehicles and provide back-up for wind and solar energy. In the present work, the $Li_4Ti_5O_{12}$-coated $LiMn_{1.5}Ni_{0.5}O_4$ material was prepared, and the structure and fast charge–discharge performance were investigated.

2. Experimental

$LiMn_{1.5}Ni_{0.5}O_4$ powders were prepared by citric acid-assisted sol–gel process. Required amounts of $CH_3COOLi \cdot 2H_2O$ (AR), $Ni(CH_3COO)_2 \cdot 4H_2O$ (AR), and $Mn(CH_3COO)_2 \cdot 4H_2O$ (AR) were dissolved in an appropriate quantity of distilled water. The solution was stirred at room temperature and the citric acid was added to the solution which acts as chelating agent in the polymeric matrix. The pH of the solution was adjusted to 7.0 by slowly dropping ammonium hydroxide dropwise and continued stirring for 4 h. The temperature of the solution was raised to about 80 °C and stirring continued till the solution turned into highly viscous gel. The resulted gel was dried at 120 °C for 24 h. The precursor powder was ground to fine powder and sintered at 450 °C under air flowing conditions with a constant heating followed by cooling at rate 5 °C min^{-1} to decompose organic constituents. The sintered powder was ground to a fine powder and re-sintered successively at 800 °C for 12 h and heating and cooling rate was maintained at 5 °C min^{-1}.

LTO-coated $LiMn_{1.5}Ni_{0.5}O_4$ materials were synthesized by the following way. $Ti(C_4H_9O)_4$ (AR) and $CH_3COOLi \cdot 2H_2O$ with a stoichiometric cationic ratio were dissolved in a solution containing ethanol and distilled water to form a clear solution. Then citric acid was added into the above solution with stirring to obtain a sol. The as-prepared $LiMn_{1.5}Ni_{0.5}O_4$ was slowly added to the above sol under stirring. After hydrolyzing for 5 h, a black gel formed. Finally, the gelatin was dried at 100 °C for 1 h and fired at 750 °C for 5 h to obtain the final powders.

Differential thermal analysis (DTA) and thermogravimetery (TG) measurements were performed in air from room temperature to 840 °C with a HCT-1/2 thermal analysis system (Beijing, China) under a scanning rate of 5 °C min^{-1}. The phase purity was verified from powder X-ray diffraction (XRD) measurements. The particle morphology of the powders after sintering was obtained using a scanning electron microscopy (SEM). The cyclic voltammetry (CV) test was carried out on a CHI-852C electrochemical workstation with a voltage between 3.3 and 5.0 V at a scanning rate of 0.15 mV s^{-1}. Charge–discharge measurements were carried out at different C-rates over the potential range of 3.3–4.95 (versus Li/Li^+) using a Land 2000T (China) battery tester at room temperature.

Electrochemical performance was carried out with a CR 2032 coin cell. The candidate cathode material was mixed with 10 wt% polyvinylidene fluoride (PVDF) binder and 10 wt% carbon black in N-methyl-2-pyrrolidone (NMP) into homogeneous slurry. The resulting paste was cast on an aluminum current collector. The coin cell was made using $Li_4Ti_5O_{12}$-coated $LiMn_{1.5}Ni_{0.5}O_4$ as a cathode, lithium metal foil as an anode, Celgard 2300 as separators and 1 M $LiPF_6$ as in EC:DMC = 1:1 (volume ratio) solvent used as an electrolyte, and assembled in an argon-filled glove box.

3. Results and discussion

In lithium salt–nickel salt–citric acid–water system, the possible precipitates are taken to be LiOH(s) and $Ni(OH)_2$(s). In this system, the LiOH(s) is highly soluble in an aqueous solution that it can be precipitated only in a fairly basic region (pH > 13) [24]. The solubility of Li^+ can be expected to be increased because it can form the soluble citrate complexes such as $LiC_6H_5O_7^{2-}$ in the citric acid solution. $Ni(OH)_2$ can be precipitated only at the pH value above 7.1 in the aqueous solution. In fact, the Ni^{2+} cannot be precipitated in citric acid solution, because it can form the citric acid nickel (II) complex. The complexation process is as follows:

$$2C_6H_8O_7 + 3Ni^{2+} \rightarrow C_{12}H_{10}Ni_3O_{14} + 6H^+ \quad (1)$$

Hence, it can be concluded that the precipitates do not contain LiOH(s) and $Ni(OH)_2$(s). The bivalent manganese (Mn^{2+}) ions can hydrolyze to the $Mn(OH)_2$(s) precipitate at around pH 6.0 in an aqueous solution. Fig. 1. shows the

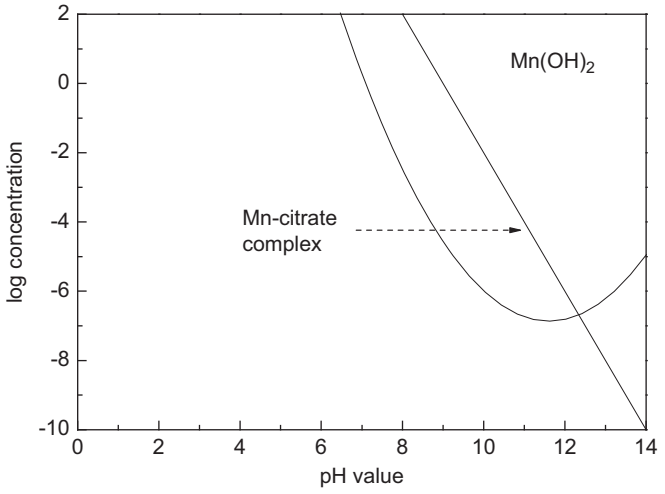

Fig. 1. Isotherm for the $Mn(OH)_2$–citric acid–water system from Refs. [24,25].

isotherm for the $Mn(OH)_2$–citric acid–water system from Refs. [24,25]. From Fig. 1, it can been seen that the $Mn(OH)_2$ begins to form precipitates around pH 8.0, since citric acid takes part in the complex formation of manganese salt in the manganese salt–citric acid–water system [24]. On the other hand, taking into account the dissociation of citric acid, it is desirable to work at $pH > pK_3$ (6.4) [26] for ensuring the complete dissociation of citric acid. In this regard, the optimum pH for the synthesis of pure and stable metal citrate complexes may be determined to be 6.4–8.0, where the formation of impurity phases such as hydroxides is effectively suppressed. Hence, the pH value of the solution is determined to be 7.0.

Fig. 2 shows the TG–DTA curves of the precursor for $LiMn_{1.5}Ni_{0.5}O_4$ samples. From the TG curve, it can be seen that a step-wise weight loss in the temperature ranges from 25 to 145 °C, 145 to 223 °C, 223 to 283 °C, and 283 to 402 °C. The least weight loss in the first region may be attributed to the superficial water loss on the gel precursor due to the hygroscopic nature of the precursor complex [27]. The second weight loss can be associated with the loss of crystal water in the reagents of the mixed precursor. The third weight loss may be due to the thermal acetate decomposition. In the last region, an intensive exothermic peak observed at 317 °C is accompanied by noticeable weight lose in the TG curve. About 47.6 wt% of the weight loss occurs during this stage because of a violent oxidation–decomposition reaction. It is due to the decomposition of the inorganic and the organic constituents of the precursor followed by the preliminary formation of $LiMn_{1.5}Ni_{0.5}O_4$ compounds. It appears that citric acid functions as a fuel in the decomposition of the acetate ions. The evolving heat resulting from the decomposition of acetate ions accelerates the decomposition of the remaining organic constituents. This may improve the crystallization reaction of $LiMn_{1.5}Ni_{0.5}O_4$ compound. Above 400 °C, there is almost no weight loss observed in the TG curve, indicating that water and most organic groups have been removed, and that any further heating only makes the crystalline phase of samples more perfect.

The XRD patterns of the as-prepared LTO-coated $LiMn_{1.5}Ni_{0.5}O_4$ are presented in Fig. 3. The main diffraction peaks for the samples can be indexed to a cubic spinel $LiMn_2O_4$ structure with a minor impurity. The sharp peaks in the pattern show good crystallinity of the cathode. As shown in Fig. 3, a small amount impurities close to the (4 0 0) characteristic peak are observed in XRD patterns of all samples, and this can be assigned to $Li_xNi_{1-x}O$ or NiO [28,29]. It has been reported that an impurity phase ($Li_xNi_{1-x}O$) can be formed at annealing temperatures above 750 °C in $LiMn_{1.5}Ni_{0.5}O_4$ [30]. Amine et al. [31] have reported that $LiMn_{1.5}Ni_{0.5}O_4$ loses oxygen and disproportionates to a spinel and rock salt NiO when it is heated above 600 °C. The lattice parameter calculated through the least squares program method from the diffraction data of $LiMn_{1.5}Ni_{0.5}O_4$ is agreed well with those of other research groups [32,33]. From Fig. 3, it is

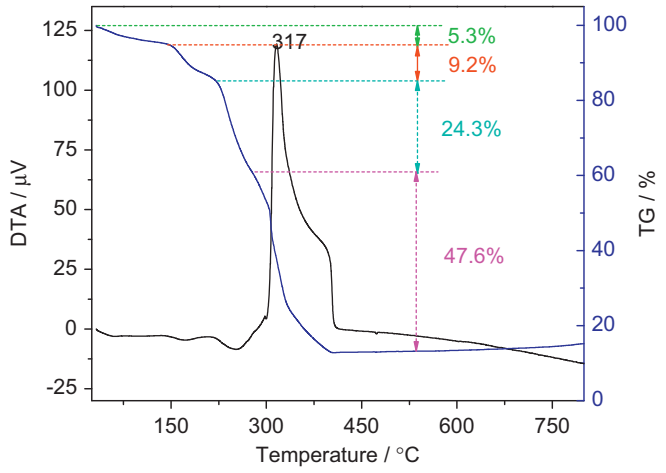

Fig. 2. TG–DTA curves for the thermal decomposition of the precursor $LiMn_{1.5}Ni_{0.5}O_4$ synthesized by sol–gel method.

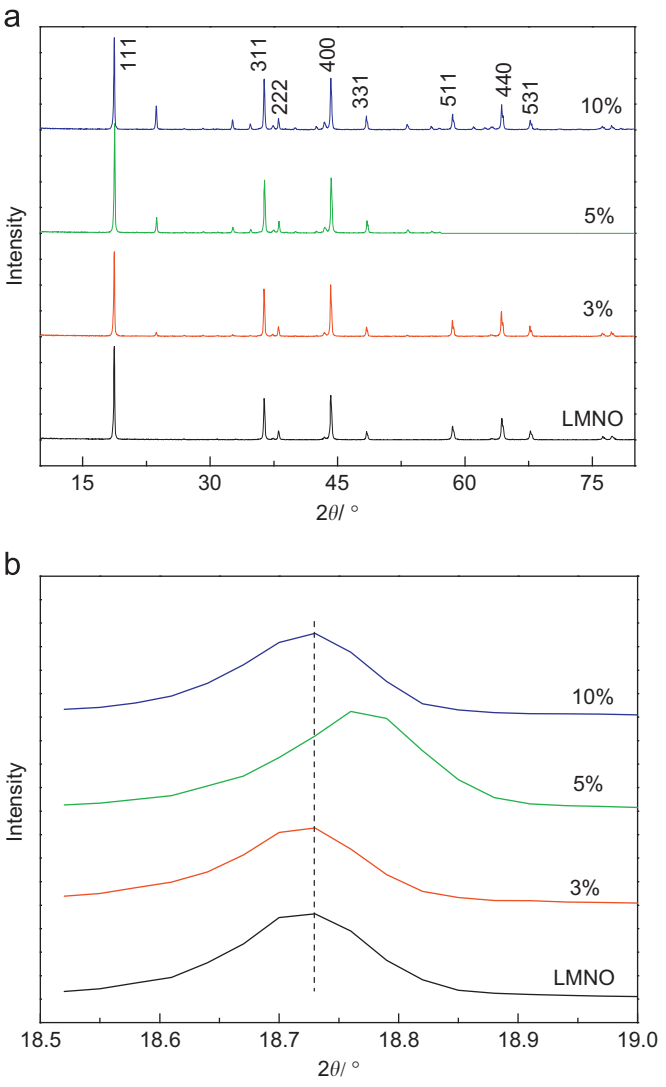

Fig. 3. XRD patterns of (a) LTO-coated $LiMn_{1.5}Ni_{0.5}O_4$ with different contents and (b) enlarged (1 1 1) peaks for the coated materials.

confirmed that 3 wt% LTO-coated materials expose the absence of secondary phase peaks except for $Li_xNi_{1-x}O$ in the range of the diffraction patterns. This may be attributed to the very low concentrations of LTO. However, distinct additional peaks start appearing in the diffractograms of 5 wt% and 10 wt% LTO-coated materials. The reason may be that a substitutional compound ($TiMnO_3$) may be formed when treated at a high temperature. From the enlargement of the XRD patterns of Fig. 3, it can be seen that the diffraction patterns of the 5 wt% and 10 wt% LTO-coated $LiMn_{1.5}Ni_{0.5}O_4$ shift toward higher angles compared to those of pure $LiMn_{1.5}Ni_{0.5}O_4$, showing that the lattice constants *a* decreases. The reason may be that Ti^{4+} ions enter the crystal lattice of $LiMn_{1.5}Ni_{0.5}O_4$ during the high coating process. Hence, it can be concluded that a substitutional compound $LiMn_{2-x-y}Ni_xTi_yO_4$ has formed through the interaction of the coated oxide with the substrate. This can be compared with the TiO_2-coated $LiCoO_2$ [34] and LTO-coated $LiCoO_2$ [35]. These variations are attributed to the ionic radius differences among Li^+ (0.59 Å), Ni^{2+}(0.69 Å), Mn^{4+} (0.53 Å), and Ti^{4+} (0.605 Å) [36], revealing the incorporation of Ti atoms onto the Ni sites.

Fig. 4 depicts the SEM micrographs of the pristine and LTO-coated $LiMn_{1.5}Ni_{0.5}O_4$. The surface morphology of the pristine $LiMn_{1.5}Ni_{0.5}O_4$ is smooth and clean (Fig. 4a). On the other hand, the surface of the coated $LiMn_{1.5}Ni_{0.5}O_4$ is covered with small particles that consist mainly of LTO, as shown in Fig. 4(b) and (c). From a comparison of these three powders surface morphologies, it can be speculated that the surface of the prepared $LiMn_{1.5}Ni_{0.5}O_4$ is covered with small LTO [37].

Typical cyclic voltammograms of pristine and 3 wt% LTO-coated $LiMn_{1.5}Ni_{0.5}O_4$ are shown in Fig. 5. The appearance of about 4 V peak is due to Mn^{3+} ions which are formed by the oxygen loss during high temperature calcinations. The difference in the voltage plateau could be used to identify if the spinel material is ordered or disordered. A small step appearing around 4 V in the disordered material was associated with the Mn^{3+}/Mn^{4+} redox couple [38,39]. Hence, it can be concluded that our prepared pristine and 3 wt% LTO-coated $LiMn_{1.5}Ni_{0.5}O_4$ has disordered spinel structure with Fd-3m space group. The two major peaks appearing between 4.5 and 5 V during charge and discharge cycling were due to the two-step oxidation/reduction of Ni^{2+}/Ni^{3+} and Ni^{3+}/Ni^{4+} [40,41]. However, the two cathodic and anodic peaks of 3 wt% LTO-coated $LiMn_{1.5}Ni_{0.5}O_4$ overlapped to a broad peak because of very narrow potential gap between peaks and look like one broad peak [42]. The potential difference (φ_a–φ_c) between anodic and cathodic peaks can reflect the polarization degree of the electrode. The potential difference (φ_a–φ_c) of 3 wt% LTO-coated $LiMn_{1.5}Ni_{0.5}O_4$ electrode is lower than that of pure $LiMn_{1.5}Ni_{0.5}O_4$, suggesting that the former has a faster lithium insertion/extraction kinetics than that of the latter. This observation confirms that the LTO-coating enhances the reversibility of the $LiMn_{1.5}Ni_{0.5}O_4$, and LTO-coated $LiMn_{1.5}Ni_{0.5}O_4$ electrode has a good reversibility and a good rate capability.

Although a number studies focused on high rate discharge of $LiMn_{1.5}Ni_{0.5}O_4$ material obtained at various temperatures, there were few reports on the fast charge–discharge performance. In spite of the fact that the high rate charge performance was an important factor to evaluate the electrochemical performance of the materials, previous studies ignored this issue. When the electrochemical performances of different cathode materials are compared, charge performance is very important especially at high C-rates. Hence, the fast charge–discharge is very important during the practical commercial application especially for power battery. Fig. 6 shows the room

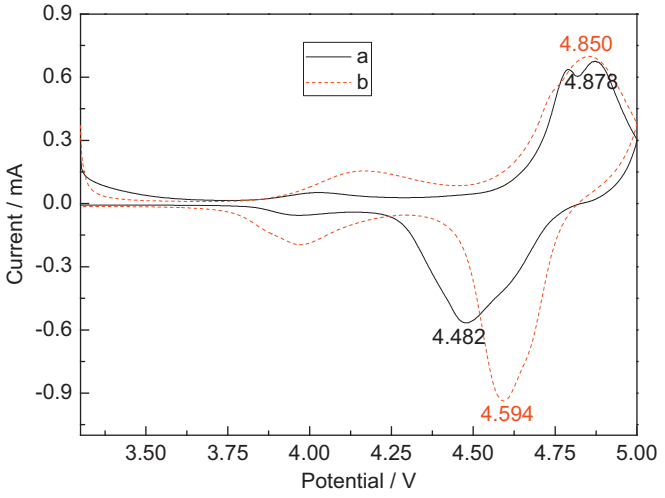

Fig. 5. Cyclic voltammograms of LTO-coated $LiMn_{1.5}Ni_{0.5}O_4$ cells with different contents: (a) 0 wt% and (b) 3 wt% between 3.3 and 5 V.

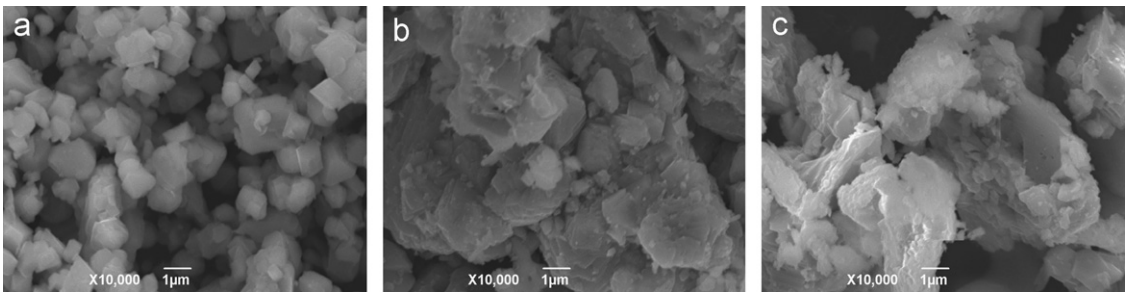

Fig. 4. SEM micrographs of LTO-coated $LiMn_{1.5}Ni_{0.5}O_4$ with different contents: (a) 0 wt%, (b) 3 wt% and (c) 5 wt%.

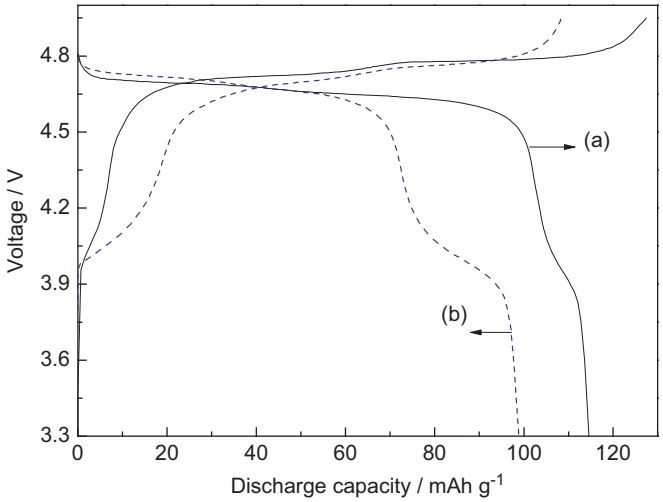

Fig. 6. Initial charge–discharge curves of (a) $LiMn_{1.5}Ni_{0.5}O_4$ and (b) 3 wt% LTO-coated $LiMn_{1.5}Ni_{0.5}O_4$ charge–discharged at 0.5 C rate.

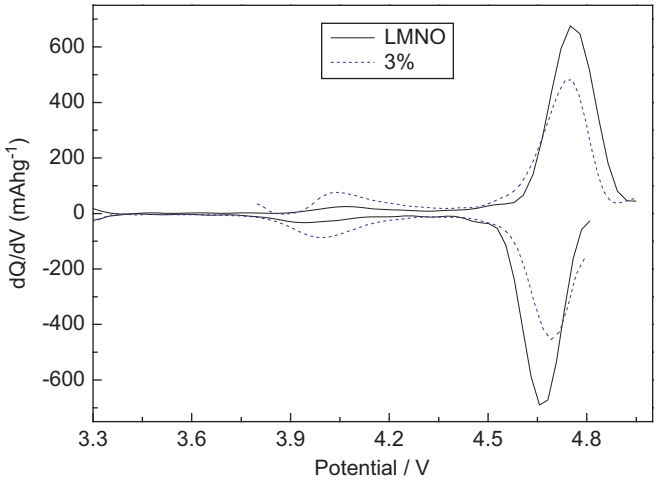

Fig. 7. Differential capacity versus voltage plots of $LiMn_{1.5}Ni_{0.5}O_4$ and 3 wt% LTO-coated $LiMn_{1.5}Ni_{0.5}O_4$ in 3.3–4.95 V range.

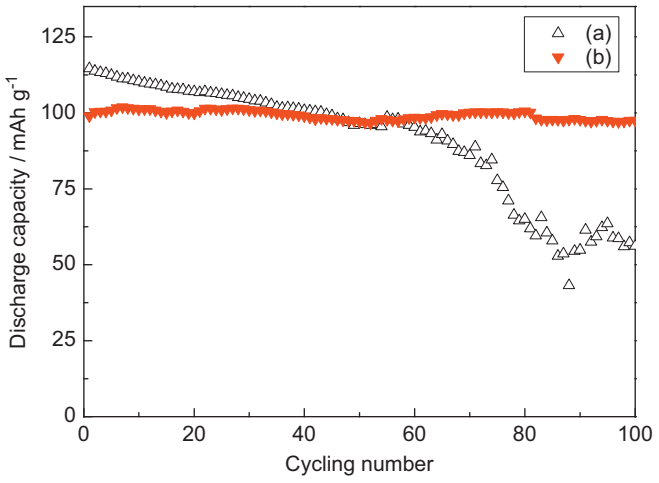

Fig. 8. Cyclic performance of LTO-coated $LiMn_{1.5}Ni_{0.5}O_4$ with different contents at 0.5 C charge–discharge rate: (a) 0 wt% and (b) 3 wt%.

temperature charge–discharge characteristics of coin cells carried out galvanostatically between 3.3 and 4.95 V at 0.5 C charge–discharge rates.

It can be found that there are two unambiguous plateaus in the charge–discharge curves of pristine and modified $LiMn_{1.5}Ni_{0.5}O_4$. The plateau at around 4.0 V is due to the redox reaction of the small amounts of Mn^{3+} ions present in the samples. The potential plateau at 4.7 V corresponds to the Ni^{4+}/Ni^{2+} redox reaction. The initial discharge capacities of pristine $LiMn_{1.5}Ni_{0.5}O_4$ and 3 wt% LTO-coated $LiMn_{1.5}Ni_{0.5}O_4$ are 115 and 109 mA h g^{-1}, respectively. The coated material shows a low discharge capacity. The reason may be that the coating layer hinders the extraction and insertion of lithium ion from the cathode during charge–discharge process and results in the low initial capacity [43]. In addition, the coated material shows a low charge voltage compared with the pristine $LiMn_{1.5}Ni_{0.5}O_4$. This indicates that the LTO coating reduces the polarization during charge, and then exhibits a batter charge acceptance than that of pristine $LiMn_{1.5}Ni_{0.5}O_4$.

Fig. 7 shows the plots of dQ/dV versus voltage for the pristine and 3 wt% LTO-coated $LiMn_{1.5}Ni_{0.5}O_4$ cathode from Fig. 6. It can be seen that the voltage gap between charge and discharge peaks of pristine $LiMn_{1.5}Ni_{0.5}O_4$ is obviously larger than that of LTO-coated one. It can be concluded that the LTO coating layer is very helpful to improve the reversibility of lithium insertion/extraction.

Fig. 8 shows the cycling performance of 3 wt% LTO-coated and uncoated $LiMn_{1.5}Ni_{0.5}O_4$ at 0.5 C charge–discharge rate. As for uncoated $LiMn_{1.5}Ni_{0.5}O_4$, the specific discharge capacity fades to 56.2 mA h g^{-1} at the 100th cycle with a capacity retention ratio of 48.9%. In the case of LTO-coated materials, the discharge capacity at the 100th cycle decreases to 97.5 mA h g^{-1} with capacity retention ratio of 89.5%. Obviously the LTO coating shows a positive effect on improving the cycling performance of $LiMn_{1.5}Ni_{0.5}O_4$. The reason for this may be as follows. It has been reported that HF can be generated during cycling when using $LiPF_6$-based electrolyte [44,45]. The electrolyte decomposition by water traces is as follows [45]:

$$LiPF_6 + H_2O \rightarrow POF_3 + LiF + 2HF \quad (2)$$

The HF could attack cathode material to cause the transitional metal to dissolve. The coated LTO layer on the surface of $LiMn_{1.5}Ni_{0.5}O_4$ suppresses transitional metal dissolution and increases the structural stability. Hence, this improvement can be attributed to minimization of the side reactions between the cathode and electrolyte by the LTO protecting layer during cycling.

The beneficial effect of LTO reached not only specific capacity, but also coulombic efficiency. The coulomb efficiency of 3 wt% LTO-coated and uncoated $LiMn_{1.5}Ni_{0.5}O_4$ charge–discharged at 0.5 C rate in the voltage range of 3.3–4.95 V is given in Fig. 9. The efficiency is defined as the discharge capacity divided by the charge capacity in one charge/discharge cycle. It can be seen that both electrodes have low coulomb efficiency in the first

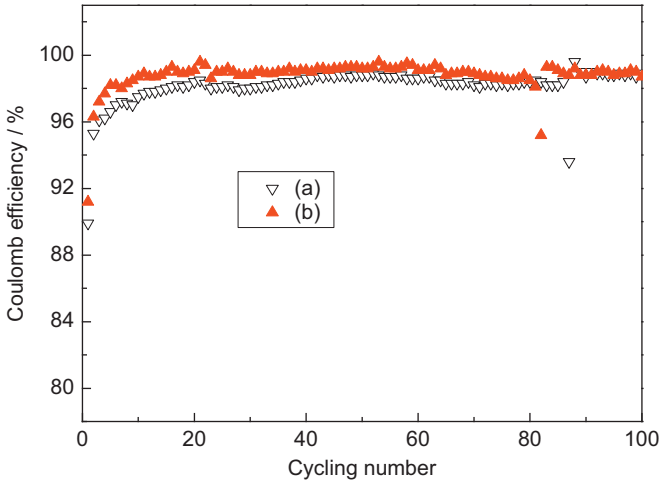

Fig. 9. Coulombic efficiency of (a) $LiMn_{1.5}Ni_{0.5}O_4$ and (b) 3 wt% LTO-coated $LiMn_{1.5}Ni_{0.5}O_4$ charge–discharged at 0.5 C rate between 3.3 and 4.95 V.

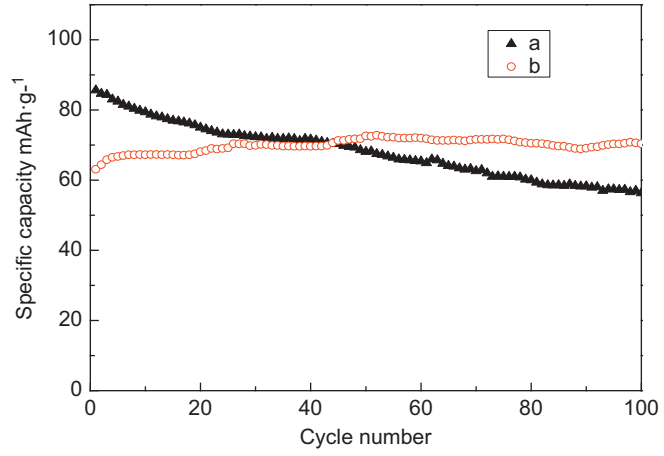

Fig. 10. Cycling performance of (a) $LiMn_{1.5}Ni_{0.5}O_4$ and (b) 3 wt% LTO-coated $LiMn_{1.5}Ni_{0.5}O_4$ charge–discharged at 1 C rate between 3.3 and 4.95 V.

charge–discharge cycle due to the electrolyte decomposition at high voltage. After about 15 cycles, the coulomb efficiency of both electrodes arrives at 98%. The improved efficiency can be attributed to the formation of protection layer on the electrode surface. It is obvious that the 3 wt% LTO-coated electrode has a higher average value of coulomb efficiency than that of the $LiMn_{1.5}Ni_{0.5}O_4$ electrode, implying that the coating is beneficial to the reversible intercalation and de-intercalation of Li^+.

Fig. 10 compares the high rate cycling performance of pristine and 3 wt% LTO-coated and uncoated $LiMn_{1.5}Ni_{0.5}O_4$ charge–discharged at 1 C rates. Compared with Fig. 8, the discharge capacities of both electrodes significantly decrease when the charge–discharge currents are 1 C. For example, the capacity reaches only 70.4 mA h g^{-1} at 1 C charge–discharge rate, which is only 72.2% of the 0.5 C rate. Geng et al. [46] reported that the overpotential contributed from the charge-transfer reaction and diffusion can be easily derived from the anodic polarization results, and high-rate discharge ability was mainly controlled by the diffusion behavior rather than by the charge-transfer reaction [46,47]. Hence, the diffusion overpotential is lower than the charge-transfer overpotential at low discharge current densities but becomes more dominant at higher current densities [48]. This explains the large capacity drop. Though pristine $LiMn_{1.5}Ni_{0.5}O_4$ exhibits a higher initial discharge capacity than that of 3 wt% LTO-coated $LiMn_{1.5}Ni_{0.5}O_4$, the latter shows a higher discharge capacity than that of the former after 43 cycles. As shown in Fig. 10, after 100 cycles, the discharge capacity of the 3 wt% LTO-coated $LiMn_{1.5}Ni_{0.5}O_4$ still remains 100% of original values, indicating a high utility of electric capability. Therefore, surface modification by LTO is an effective way to improve the fast charge–discharge performance of $LiMn_{1.5}Ni_{0.5}O_4$ cathode materials for lithium-ion batteries.

4. Conclusions

Pristine and LTO-coated $LiMn_{1.5}Ni_{0.5}O_4$ were successfully prepared by a sol–gel method followed by high-temperature calcinations. The surface coating of LTO is beneficial to the reversible intercalation and de-intercalation of Li^+. The 3 wt% LTO-coated $LiMn_{1.5}Ni_{0.5}O_4$ exhibits excellent fast charge–discharge performances. The 3 wt% LTO-coated $LiMn_{1.5}Ni_{0.5}O_4$ shows a high reversible capacity of more than 97 mA h g^{-1} after 100 cycles at a current density of 0.5 C, as well as more stable cycle performance and better rate capability, than the bare $LiMn_{1.5}Ni_{0.5}O_4$. The discharge capacity of the 3 wt% LTO-coated $LiMn_{1.5}Ni_{0.5}O_4$ still remains 100% of original values at 1 C charge–discharge rate after 100 cycles. This improvement is attributed to minimization of the side reactions between the cathode and electrolyte by the LTO protecting layer. Therefore, the presence of an LTO layer between the electrolyte and the active material plays a beneficial role in increasing both the cycling efficiency and the rate capability of $LiMn_{1.5}Ni_{0.5}O_4$ electrodes. It can be concluded that LTO-coated $LiMn_{1.5}Ni_{0.5}O_4$ provides a great prospect for practical applications in commercial rechargeable lithium batteries due to the enhanced fast charge–discharge ability and cycling stability.

Acknowledgments

This work was financially supported by the National Natural Science Foundation of China (Grant Nos. 51274002 and 50902001), the Key project of Scientific Research Foundation sponsored by Education Department of Anhui Province, China (No. KJ2010A045), and the Program for Innovative Research Team in Anhui University of Technology No. (TD201202).

References

[1] J. Yang, S.C. Wang, X.Y. Zhou, J. Xie, Electrochemical behaviors of functionalized carbon nanotubes in $LiPF_6$/EC+DMC electrolyte, International Journal of Electrochemical Science 7 (2012) 6118–6126.

[2] J. Yang, X.Y. Zhou, Y.L. Zou, J.J. Tang, A hierarchical porous carbon material for high power, lithium ion batteries, Electrochimica Acta 56 (2011) 8576–8581.

[3] M. Wohlfahrt-Mehrens, C. Vogler, J. Garche, Aging mechanisms of lithium cathode materials, Journal of Power Sources 127 (2004) 58–64.

[4] G.G. Amatucci, C.N. Schmutz, A. Blyr, C. Sigala, A.S. Gozdz, D. Larcher, J.M. Tarascon, Materials' effects on the elevated and room temperature performance of C/$LiMn_2O_4$ Li-ion batteries, Journal of Power Sources 69 (1997) 11–25.

[5] Y. Xia, Y. Zhou, M. Yoshio, Capacity fading on cycling of 4 V Li / $LiMn_2O_4$ cells, Journal of the Electrochemical Society 144 (1997) 2593–2600.

[6] N.M. Hagh, G.G. Amatucci, A new solid-state process for synthesis of $LiMn_{1.5}Ni_{0.5}O_{4-\delta}$ spinel, Journal of Power Sources 195 (2010) 5005–5012.

[7] Y.P. Fu, Y.H. Su, S.H. Wu, C.H. Lin, $LiMn_{2-y}M_yO_4$ (M=Cr, Co) cathode materials synthesized by the microwave-induced combustion for lithium ion batteries, Journal of Alloys and Compounds 426 (2006) 228–234.

[8] R. Thirunakaran, A. Sivashanmugam, S. Gopukumar, C.W. Dunnill, D.H. Gregory, Phthalic acid assisted nano-sized spinel $LiMn_2O_4$ and $LiCr_xMn_{2-x}O_4$ (x=0.00–0.40) via sol–gel synthesis and its electrochemical behaviour for use in Li-ion-batteries, Materials Research Bulletin 43 (2008) 2119–2129.

[9] J.M. Lloris, B. León, C. Pérez Vicente, J.L. Tirado, M. Womes, J. Olivier Fourcade, J.C. Jumas, Composition and electrochemical properties of $LiCu_xMn_{2-x}O_4$ and $LiCu_{0.5-y}Al_yMn_{1.5}O_4$, Journal of Solid State Electrochemistry 8 (2004) 521–525.

[10] J. Molenda, J. Marzec, K. Świerczek, D. Pałubiak, W. Ojczyk, M. Ziemnicki, The effect of 3d substitutions in the manganese sublattice on the electrical and electrochemical properties of manganese spinel, Solid State Ionics 175 (2004) 297–304.

[11] P.V. Braun, J. Cho, J.H. Pikul, W.P. King, H. Zhang, High power rechargeable batteries, Current Opinion in Solid State and Materials Science 16 (2012) 186–198.

[12] D. Aubarch, A. Zaban, A. Schlecter, Y. Ein-Eli, E. Zinigrad, B. Markowsky, The study of electrolyte solutions based on ethylene and diethyl carbonates for rechargeable Li batteries: I. Li metal anodes, Journal of the Electrochemical Society 142 (1995) 2873–2882.

[13] D.H. Jang, S.M. Oh, Electrolyte effects on spinel dissolution and cathodic capacity losses in 4 V Li/$Li_xMn_2O_4$ rechargeable cells, Journal of the Electrochemical Society 144 (1997) 3342–3348.

[14] H. Sclar, O. Haik, T. Menachem, J. Grinblat, N. Leifer, A. Meitav, S. Luski, D. Aurbach, The effect of ZnO and MgO coatings by a sono-chemical method, on the stability of $LiMn_{1.5}Ni_{0.5}O_4$ as a cathode material for 5 V Li-ion batteries, Journal of the Electrochemical Society 159 (2012) (2012) A228–A237.

[15] J. Liu, A. Manthiram, Kinetics study of the 5 V spinel cathode $LiMn_{1.5}Ni_{0.5}O_4$ before and after surface modifications, Journal of the Electrochemical Society 156 (2009) A833–A838.

[16] J.S. Kim, C.S. Johnson, J.T. Vaughey, S.A. Hackney, K.A. Walz, W.A. Zeltner, M.A. Anderson, M.M. Thackeray, The electrochemical stability of spinel electrodes coated with ZrO_2, Al_2O_3, and SiO_2 from colloidal suspensions, Journal of the Electrochemical Society 151 (2004) A1755–A1761.

[17] Y. Fan, J. Wang, Z. Tang, W. He, J. Zhang, Effects of the nanostructured SiO_2 coating on the performance of $LiNi_{0.5}Mn_{1.5}O_4$ cathode materials for high-voltage Li-ion batteries, Electrochimica Acta 52 (2007) 3870–3875.

[18] Y. Kobayashi, H. Miyashiro, K. Takei, H. Shigemura, M. Tabuchi, H. Kageyama, T. Iwahori, 5 V class all-solid-state composite lithium battery with Li_3PO_4 coated $LiNi_{0.5}Mn_{1.5}O_4$, Journal of the Electrochemical Society 150 (2003) A1577–A1582.

[19] T.Y. Yang, N.Q. Zhang, Y. Lang, K.N. Sun, Enhanced rate performance of carbon-coated $LiNi_{0.5}Mn_{1.5}O_4$ cathode material for lithium ion batteries, Electrochimica Acta 56 (2011) 4058–4064.

[20] T. Ohzuku, A. Ueda, N. Yamamoto, Zerostrain insertion material of $Li[Li_{1/3}Ti_{5/3}]O_4$ for rechargeable lithium cells, Journal of the Electrochemical Society 142 (1995) 1431–1435.

[21] T.F. Yi, L.J. Jiang, J. Shu, C.B. Yue, R.S. Zhu, H.B. Qiao, Recent development and application of $Li_4Ti_5O_{12}$ as anode material of lithium ion battery, Journal of Physics and Chemistry of Solids 71 (2010) 1236–1242.

[22] K. Takada, N. Ohta, L. Zhang, K. Fukuda, I. Sakaguchi, R. Ma, M. Osada, T. Sasaki, Interfacial modification for high-power solid-state lithium batteries, Solid State Ionics 179 (2008) 1333–1337.

[23] D.Q. Liu, J. Yu, Y.H. Sun, Z.Z. He, X.Q. Liu, Preparation and rate property of $Li_4Ti_5O_{12}$-coated $LiMn_2O_4$ for lithium ion battery, Chinese Journal of Inorganic Chemistry 23 (2007) 41–45.

[24] J.H. Choy, D.H. Kim, C.W. Kwon, S.J. Hwang, Y.I. Kim, Physical and electrochemical characterization of nanocrystalline $LiMn_2O_4$ prepared by a modified citrate route, Journal of Power Sources 77 (1999) 1–11.

[25] T.F. Yi, C.S. Dai, K. Gao, X.G. Hu, Effects of synthetic parameters on structure and electrochemical performance of spinel lithium manganese oxide by citric acid-assisted sol–gel method, Journal of Alloys and Compounds 425 (2006) 343–347.

[26] J.H. Choy, Y.S. Han, Citrate route to the piezoelectric Pb(Zr,Ti)O_3 oxide, Journal of Materials Chemistry 7 (1997) 1815–1820.

[27] A. Subramania, N. Angayarkanni, T. Vasudevan, Effect of PVA with various combustion fuels in sol–gel thermolysis process for the synthesis of $LiMn_2O_4$ nanoparticles for Li-ion batteries, Materials Chemistry and Physics 102 (2007) 19–23.

[28] Q. Zhong, A. Bonakdarpour, M. Zhang, Y. Gao, J.R. Dahn, Synthesis and electrochemistry of $LiNi_xMn_{2-x}O_4$, Journal of the Electrochemical Society 144 (1997) 205–213.

[29] Y.K. Sun, C.S. Yoon, I.H. Oh, Surface structural change of ZnO-coated $LiNi_{0.5}Mn_{1.5}O_4$ spinel as 5 V cathode materials at elevated temperatures, Electrochimica Acta 48 (2003) 503–506.

[30] T.A. Arunkumar, A. Manthiram, Influence of chromium doping on the electrochemical performance of the 5 V spinel cathode $LiMn_{1.5}Ni_{0.5}O_4$, Electrochimica Acta 50 (2005) 5568–5572.

[31] K. Amine, H. Tukamoto, H. Yasuda, Y. Fujita, A new three-volt spinel $Li_{1+x}Mn_{1.5}Ni_{0.5}O_4$ for secondary lithium batteries, Journal of the Electrochemical Society 143 (1996) 1607–1613.

[32] J.M. Amarilla, R.M. Rojas, J.M. Rojo, Understanding the sucrose-assisted combustion method: effects of the atmosphere and fuel amount on the synthesis and electrochemical performances of $LiNi_{0.5}Mn_{1.5}O_4$ spinel, Journal of Power Sources 196 (2011) 5951–5959.

[33] J.C. Arrebola, A. Caballero, L. Hernán, J. Morales, Re-examining the effect of ZnO on nanosized 5 V $LiNi_{0.5}Mn_{1.5}O_4$ spinel: an effective procedure for enhancing its rate capability at room and high temperatures, Journal of Power Sources 195 (2010) 4278–4284.

[34] G.T.K. Fey, C.Z. Lu, T.P. Kumar, Y.C. Chang, TiO_2 coating for long-cycling $LiCoO_2$: a comparison of coating procedures, Surface and Coatings Technology 199 (2005) 22–31.

[35] T.F. Yi, J. Shu, Y. Wang, J. Xue, J. Meng, C.B. Yue, R.S. Zhu, Effect of treated temperature on structure and performance of $LiCoO_2$ coated by $Li_4Ti_5O_{12}$, Surface and Coatings Technology 205 (2011) 3885–3889.

[36] R.D. Shannon, Revised effective ionic radii and systematic studies of interatomic distances in halides and chalcogenides, Acta Crystallographica A32 (1976) 751–767.

[37] J. Tu, X.B. Zhao, J. Xie, G.S. Cao, D.G. Zhuang, T.J. Zhu, J.P. Tu, Enhanced low voltage cycling stability of $LiMn_2O_4$ cathode by ZnO coating for lithium ion batteries, Journal of Alloys and Compounds 432 (2007) 313–317.

[38] M. Kunduraci, G.G. Amatucci, Synthesis and characterization of nanostructured 4.7 V $Li_xMn_{1.5}Ni_{0.5}O_4$ spinels for high-power lithium-ion batteries, Journal of the Electrochemical Society 153 (2006) A1345–A1352.

[39] S. Patoux, L. Sannier, H. Lignier, Y. Reynier, C. Bourbon, S. Jouanneau, F.L. Cras, S. Martinet, High voltage nickel manganese spinel oxides for Li-ion batteries, Electrochimica Acta 53 (2008) 4137–4145.

[40] R. Santhanam, B. Rambabu, Research progress in high voltage spinel $LiNi_{0.5}Mn_{1.5}O_4$ material, Journal of Power Sources 195 (2010) 5442–5451.

[41] T.F. Yi, Y. Xie, Y.R. Zhu, R.S. Zhu, M.F. Ye, High rate micron-sized niobium-doped $LiMn_{1.5}Ni_{0.5}O_4$ as ultra high power positive-electrode material for lithium-ion batteries, Journal of Power Sources 211 (2012) 59–65.

[42] K. Takahashi, M. Saitoh, M. Sano, M. Fujita, K. Kifune, Electrochemical and structural properties of a 4.7 V-class $LiNi_{0.5}Mn_{1.5}O_4$ positive electrode material prepared with a self-reaction method, Journal of the Electrochemical Society 151 (2004) A173–A177.

[43] G. Li, Z. Yang, W. Yang, Effect of $FePO_4$ coating on electrochemical and safety performance of $LiCoO_2$ as cathode material for Li-ion batteries, Journal of Power Sources 183 (2008) 741–748.

[44] D.H. Jang, Y.J. Shin, S.M. Oh, Dissolution of spinel oxides and capacity losses in 4 V $Li/Li_xMn_2O_4$ cells, Journal of the Electrochemical Society 143 (1996) 2204–2211.

[45] H. Yamane, T. Inoue, M. Fujita, M. Sano, A causal study of the capacity fading of $Li_{1.01}Mn_{1.99}O_4$ cathode at 80 °C, and the suppressing substances of its fading, Journal of Power Sources 99 (2001) 60–65.

[46] M. Geng, J. Han, F. Feng, D.O. Northwood, Characteristics of the high-rate discharge capability of a nickel/metal hydride battery electrode, Journal of the Electrochemical Society 146 (1999) 3591.

[47] M.S. Wu, H.R. Wu, Y.Y. Wang, C.C. Wan, Effects of the stoichiometric ratio of aluminium and manganese on electrochemical properties of hydrogen storage alloys, Journal of Applied Electrochemistry 33 (2003) 619–625.

[48] M.S. Wu, P.C.J. Chiang, J.C. Lin, Electrochemical investigations on advanced lithium-ion batteries by three-electrode measurements, Journal of the Electrochemical Society 152 (2005) A47–A52.